PAPER

Effect of *α*-particle irradiation on a NdFeAs(O,F) thin film

Effect of α-particle irradiation on a NdFeAs (O,F) thin film

C Tarantini[1] , K Iida[2,3] , N Sumiya[2], M Chihara[2], T Hatano[2,3] ,
H Ikuta[2,3] , R K Singh[4] , N Newman[4] and D C Larbalestier[1]

[1] National High Magnetic Field Laboratory, Florida State University, Tallahassee, FL 32310, United States of America
[2] Department of Crystalline Materials Science, Nagoya University, Chikusa-ku, Nagoya 464-8603, Japan
[3] Department of Materials Physics, Nagoya University, Chikusa-ku, Nagoya 464-8603, Japan
[4] Materials Program, Arizona State University, Tempe, 85287 AZ, United States of America

E-mail: tarantini@asc.magnet.fsu.edu

Abstract

The effect of α-particle irradiation on a NdFeAs(O,F) thin film has been investigated to determine how the introduction of defects affects basic superconducting properties, including the critical temperature T_c and the upper critical field H_{c2}, and properties more of interest for applications, like the critical current density J_c and the related pinning landscape. The irradiation-induced suppression of the film T_c is significantly smaller than on a similarly damaged single crystal. Moreover H_{c2} behaves differently, depending on the field orientation: for $H//c$ the H_{c2} slope monotonically increases with increasing disorder, whereas for $H//ab$ it remains constant at low dose and it increases only when the sample is highly disordered. This suggests that a much higher damage level is necessary to drive the NdFeAs(O,F) thin film into the dirty limit. Despite the increase in the low temperature H_{c2}, the effects on the $J_c(H//c)$ performances are moderate in the measured temperature and field ranges, with a shifting of the pinning force maximum from 4.5 to 6 T after an irradiation of 2×10^{15} cm^{-2}. On the contrary, $J_c(H//ab)$ is always suppressed. The analysis demonstrates that irradiation does introduce point defects (PD) acting as pinning centres proportionally to the irradiation fluence but also suppresses the effectiveness of c-axis correlated pinning present in the pristine sample. We estimate that significant performance improvements may be possible at high field or at temperatures below 10 K. The suppression of the $J_c(H//ab)$ performance is not related to a decrease of the J_c anisotropy as found in other superconductors. Instead it is due to the presence of PD that decrease the efficiency of the ab-plane intrinsic pinning typical of materials with a layered structure.

Supplementary material for this article is available online

Keywords: Fe-based superconductors, irradiation, pinning properties, NdFeAs(O,F), critical current

(Some figures may appear in colour only in the online journal)

1. Introduction

Irradiation of superconductors has been performed for many years to improve our fundamental knowledge of the influence of impurity scattering on the superconducting properties and to explore whether the material performance can be improved for practical applications. For instance irradiation with neutrons, α-particles or electrons of A15 phases like V$_3$Si [1, 2], Nb$_3$Al [3], V$_3$Ge [1], Nb$_3$Sn and Nb$_3$Ge [1, 4, 5] was employed to determine the effect on T_c suppression, changes in the density of states (DOS) and in H_{c2}, variation in the gap amplitude and in the Debye temperature. More recently neutron and proton irradiation was found to favourably change the pinning landscape in order to increase both H_{c2}

and J_c in commercial Nb_3Sn wires for accelerator magnets [6, 7]. In the two-bands, two-gaps MgB_2 neutron irradiation was an effective tool to demonstrate the gap merging [8, 9], which was theoretically predicted to occur with the T_c suppression. Moreover neutron and α-particles irradiation also produces an improvement of H_{c2} and J_c in MgB_2 [10–13]. In the case of high-T_c superconductors heavy ion, proton and electron irradiation was used to investigate many theoretical aspects like weak localization and Kondo-like behaviour [14] or to study the vortex phase diagram in $YBa_2Cu_3O_{7-\delta}$ (YBCO) [15, 16]. The use of heavy ion and proton irradiations are also an efficient method to introduce strongly-correlated columnar or point defects (PD) which enhance the irreversibility field and J_c at high field and high temperature in YBCO films [17, 18] or coated conductors [19]. In Fe-based superconductors irradiation with neutrons, α-particles, proton and electrons was employed to investigate the unconventional pairing mechanisms and the gap symmetry in LaFeAs(O,F), NdFeAs(O,F), $Ba(Fe,Co)_2As_2$ and $Ba(Fe_{1-x}Ru_x)_2As_2$ [20–24]. Different types of irradiation were performed on Fe-based superconductors with the intention of introducing pinning centres: columnar defects introduced by heavy ion irradiation were particularly effective in increasing J_c in $Ba(Fe,Co)_2As_2$ [25] and $(Ba,K)Fe_2As_2$ [26]. Quite different is the effect of proton irradiation on $Ba(Fe,Co)_2As_2$ films with naturally grown correlated defects: H_{c2} was found unchanged but a high-field low-temperature J_c improvement was found in particular for $H//ab$ due to the competition between intrinsic columnar and irradiation-introduced PD [27]. Neutron irradiation on NdFeAs(O,F) single crystal [28] and polycrystalline SmFeAs(O,F) [29] enhances J_c in a wide temperature range, suppressing a fishtail effect (i.e. secondary peak in $J_c(H)$) observed before irradiation. Performance improvement was also introduced in Fe(Se,Te) films by neutron [30] and proton irradiation [31].

In this paper we will present the influence of α-particle irradiation on the superconducting properties of a high-quality NdFeAs(O,F) (Nd-1111) thin film. We will compare our results on the resistivity enhancement and T_c-suppression upon irradiation with the results of a similar experiment performed on a single crystal [21]. The unusual changes in H_{c2} and the non-monotonic variation in the material electronic mass anisotropy ($\gamma = (M/m)^{1/2} = \xi_{ab}/\xi_c$, where M and m are the effective masses along the c-axis and the parallel to the ab plane, respectively, and ξ_{ab} and ξ_c are the in-plane and out-of-plane coherence lengths, respectively) are reported. The effect of irradiation in the modification of the pinning landscape is discussed in light of the introduction of new flux pinning centres, including their role in the unexpected suppression of the intrinsic pinning typical of moderate-to-highly-anisotropic superconducting materials.

2. Experimental details

The sample under investigation is a 90 nm thick Nd-1111 thin film deposited by molecular beam epitaxy on a MgO(100) substrate at Nagoya University [32, 33]. The pristine sample

critical temperature was estimated in $T_{c,90\%} \sim 49.0$ K and the high crystalline quality of the sample was verified by x-ray diffraction using the methodology described in [34]. The sample was prepared for transport characterization with Pt contact pads and a 32 μm wide/1 mm long bridge fabricated by laser cutting. The resistivity and I–V measurements were performed in a 16 T physical property measurement system over a wide temperature range down to 10 K and in variable field orientations, while maintaining a maximum Lorentz force configuration. H_{c2} was evaluated with a 90% resistivity criterion taking into account the temperature dependence of the normal state, whereas J_c was determined from the I–V curves by a 1 μV cm^{-1} criterion. After the initial characterizations, the sample was irradiated in steps by α-particles at room temperature using a 2 MeV $4He^{2+}$ ion beam from a Tandem accelerator at the Arizona State University with subsequent transport characterization measurements carried out at Florida State University. To avoid damage to the contacts, the sample was never dismounted from the transport-measurement sample holder. The sample was irradiated three times achieving the following fluences, Φ: 4×10^{14}, 2×10^{15} and 5×10^{15} cm^{-2}. Since the estimated mean free path of α-particles in Nd-1111 is 4.2 μm [21], much larger than the film thickness, uniform irradiation damage is expected throughout the sample. Based on the changes found in the previous Nd-1111 single crystal irradiation experiment [21], the first irradiation dose was selected to achieve a T_c suppression of less than 1 K in order to assure an initial limited disorder and to verify the effectiveness of irradiation on this sample.

3. Results

3.1. Resistive transition and T_c

The resistive transitions obtained before and after irradiation are reported in figure 1. The pristine sample reveals a normal state resistivity, $\rho(55 K)$, and a residual resistivity, ρ_0 [extrapolated by fitting the normal state between 55 and 150 K with a $\rho(T) = \rho_0 + AT^m$ relation], of ~0.1 mΩ cm and ~0.04 mΩ cm, respectively. It also has a sharp transition and residual resistivity ratio [RRR = $\rho(300 K)/\rho_0$] of ~14.8. Upon irradiation, $\rho(55 K)$ (and ρ_0) progressively increases and, after the last irradiation cycle, it is about 60% (140%) larger than the pristine sample with a RRR reduced to ~6.6. Irradiation produces only a modest T_c suppression compared to a similarly irradiated single crystal (figure 2) and mild transition broadening: $T_{c,90\%}$ changes by ~3.2 K at the maximum fluence, while $T_{c,50\%}$ changes by ~3.7 K. $\Delta T_c = T_{c,90\%} - T_{c,10\%}$ varies from ~3.1 to ~3.9 K with irradiation.

3.2. H_{c2} characterization and analysis

The upper critical field H_{c2} was measured with the field aligned along the two main crystallographic directions before and after irradiation (figure 3). After the first irradiation cycle, the H_{c2} temperature dependence barely changed. At
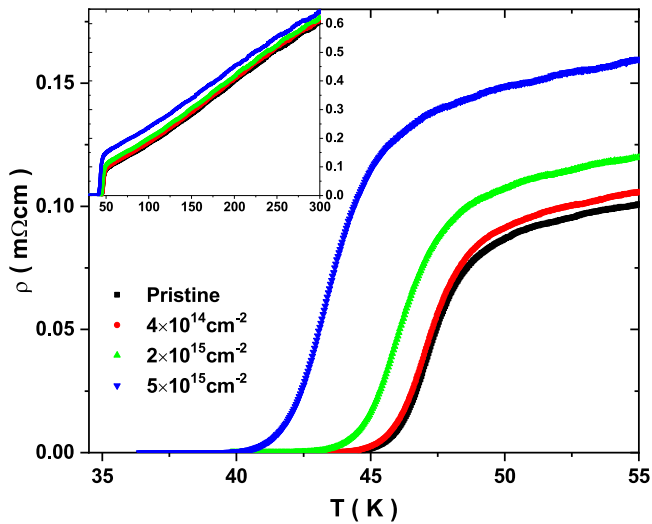
Figure 1. Resistive transition of a NdFeAs(O,F) thin film before and after irradiation with α-particles. In the main panel, a magnification of the transitions is plotted whereas the inset shows the entire temperature range of measurement.
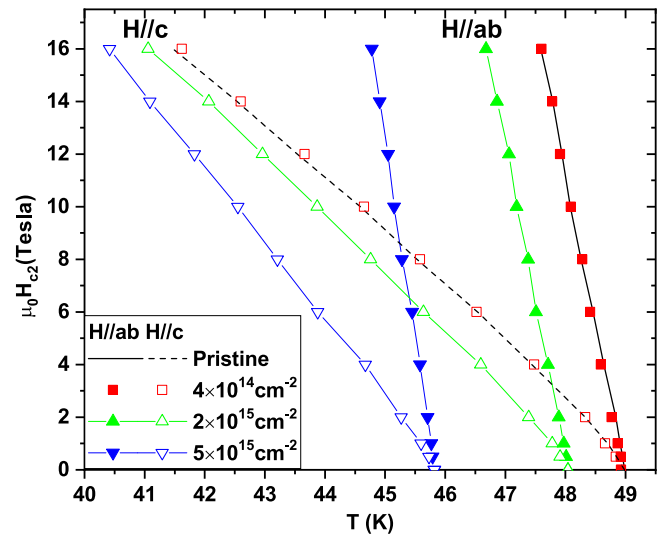

Figure 3. Temperature dependence of H_{c2} in the two main crystallographic configurations ($H//ab$, $H//c$) for a NdFeAs(O,F) thin film before and after irradiation with α-particles.
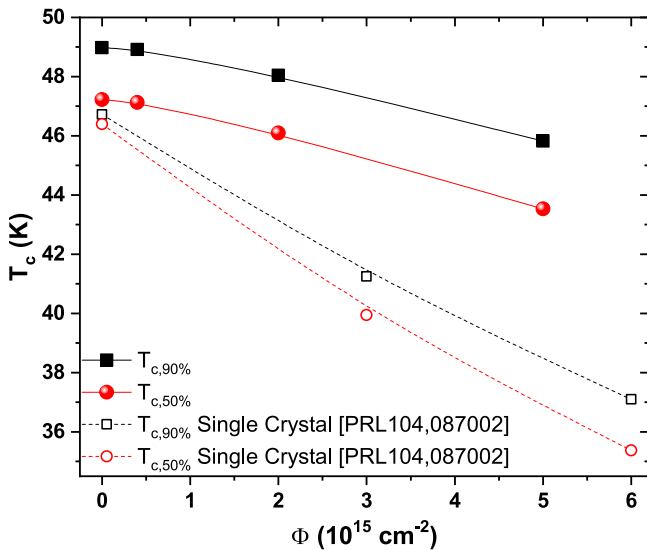

Figure 2. T_c versus fluence of α-particles for a NdFeAs(O,F) thin film. Reported trends were estimated at both 90% and 50%-criterion and compared with similar data on single crystal [21].

Figure 4. (a) H_{c2} slopes near T_c calculated from the data in figure 3 for the two main crystallographic orientations of a NdFeAs(O,F) thin film before and after irradiation with α-particles; in the inset the electronic mass anisotropy γ. (b) Coherence lengths at 0 K, $\xi_c(0)$ and $\xi_{ab}(0)$, estimated from the H_{c2} slope near T_c.

$\Phi = 2 \times 10^{15}\,\mathrm{cm}^{-2}$, $T_{c,90\%}$ was suppressed by about 1 K and $H_{c2}{}^{ab}$ appears simply shifted at lower temperatures, whereas $H_{c2}{}^{c}$ clearly shows an increase in its slope. At $\Phi = 5 \times 10^{15}\,\mathrm{cm}^{-2}$, T_c is furtherly reduced and both $H_{c2}{}^{ab}$ and $H_{c2}{}^{c}$ reveal a slope increase. In order to quantify the electronic mass anisotropy γ and to estimate the coherence lengths, the H_{c2} slopes were estimated near T_c. Because of the possible Pauli paramagnetic pair-breaking affecting H_{c2} with increasing field in Fe-based superconductors [35–37], the H_{c2} slopes were evaluated on data with $\mu_0 H \leqslant 1$ T and plotted in figure 4(a): with increasing disorder (decreasing T_c) a monotonic increase of $|\mu_0 dH_{c2}^{c}/dT|_{T_c}$ is observed while $|\mu_0 dH_{c2}^{ab}/dT|_{T_c}$ remains substantially unchanged up to the second irradiation step ($T_c \sim 48$ K) and then it suddenly

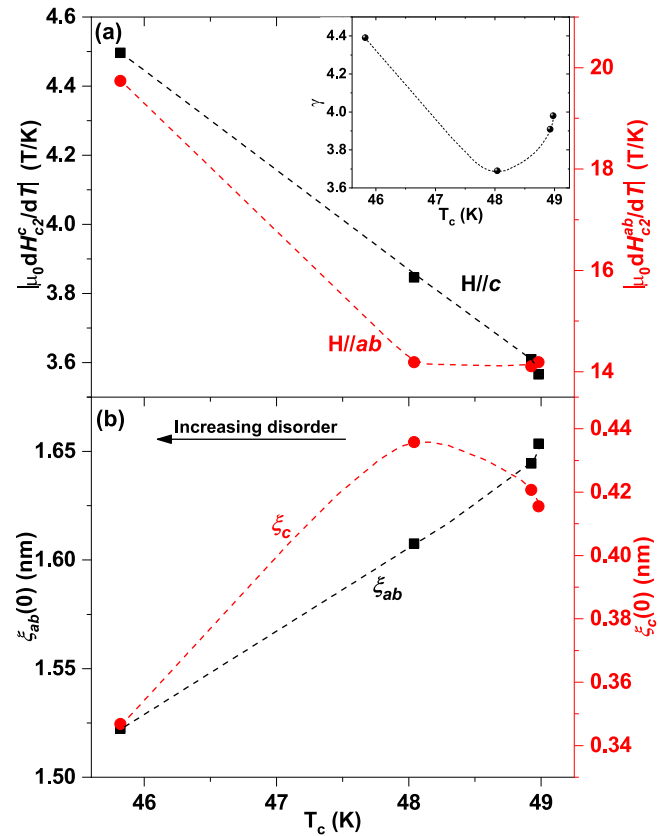increases with further disorder. As a consequence, γ has a non-monotonic trend with a minimum when T_c is ~ 48 K. The coherence lengths at 0 K, $\xi_c(0)$ and $\xi_{ab}(0)$, can be estimated from the H_{c2} slope at T_c by combining the
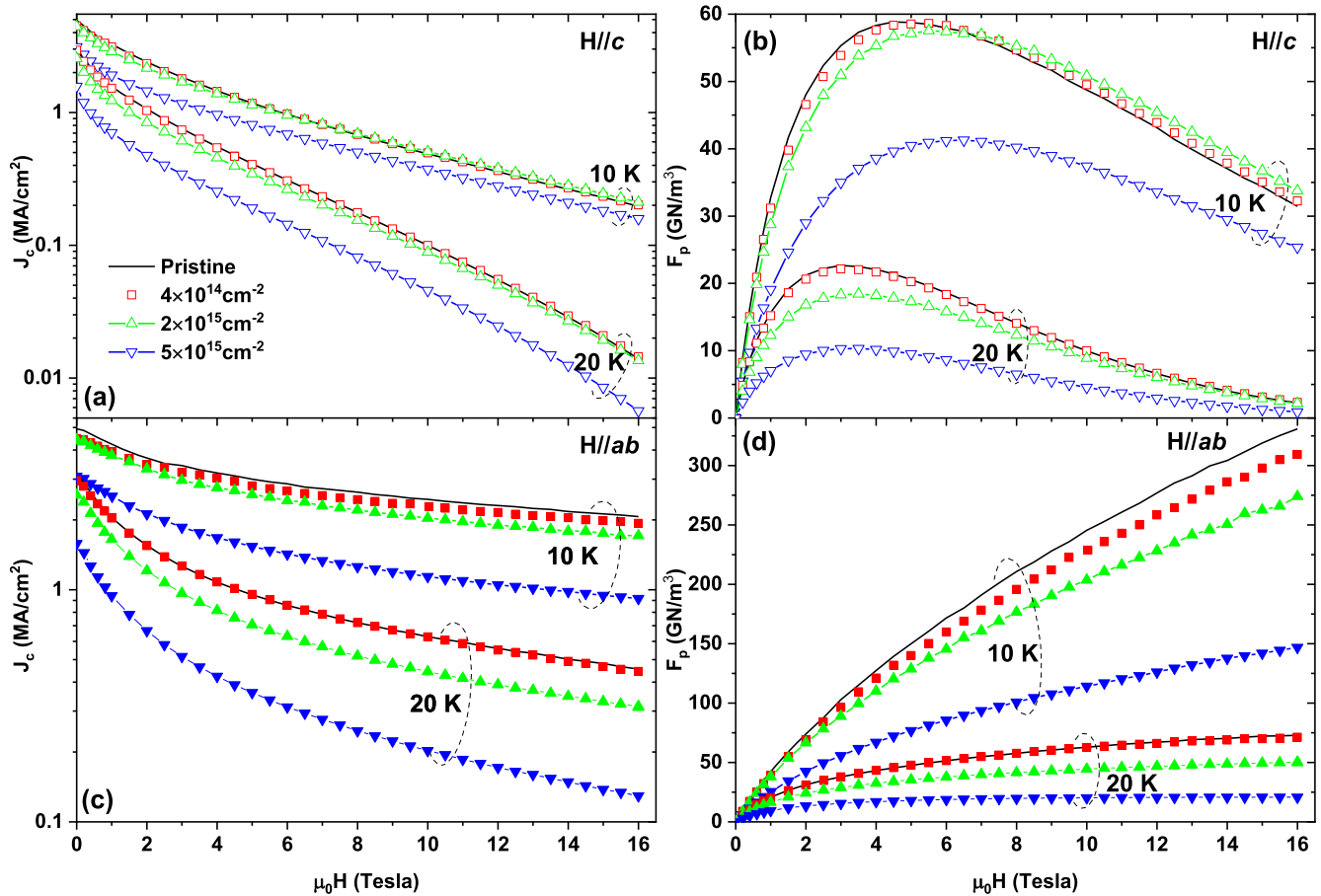
Figure 5. Field dependences of J_c and F_p at 10 and 20 K for a NdFeAs(O,F) thin film before and after irradiation with α-particles for (a), (b) $H//c$ and for (c), (d) $H//ab$.

Ginzburg–Landau expressions with the Werthamer *et al* formula [38, 39] $\xi_{ab}(0) = [\phi_0/(2\pi\mu_0 0.69T_c \, |dH_{c2}^c/dT\,|_{T_c})]^{1/2}$ and $\xi_c(0) = \xi_{ab}(0)/\gamma$. $\xi_{ab}(0)$ progressively decreases with increasing disorder, whereas $\xi_c(0)$ has a non-monotonic trend with a maximum at $T_c \sim 48$ K. It is important to notice that these estimations of ξ and γ values (obtained by single-band formulation) only provide a trend induced by irradiation damage and do not take into account the multiband nature of iron-based superconductor. In fact in multiband materials ξ and λ anisotropy parameters differ from each other and they show opposite temperature dependence merging at T_c [40]. Moreover, because of the possible paramagnetic limitation, γ and the H_{c2} anisotropy, $\gamma_{H_{c2}}$, are identical near T_c but they may differ at lower temperature [34].

3.3. J_c characterization and analysis

J_c was measured from T_c down to 10 K using 5 K increments at low temperatures and 2.5 K steps near T_c for the as-grown sample and then after irradiation. Figure 5 shows the data at 10 and 20 K as an example. In the pristine sample the self-field J_c(10 K) is $\sim$5 MA cm^{-2}, whereas the J_c(16 T, 10 K) values are just below 0.2 MA cm^{-2} and more than 2 MA cm^{-2} for $H//c$ and $H//ab$, respectively. The pinning force density F_p(10 K, $H//c$) reaches a maximum of

58.9 GN m^{-3} at 4.5 T, whereas along the *ab*-planes the maximum exceeds 300 GN m^{-3} which occurs above 16 T, outside the measurement range. After irradiation a small increase of $J_c(H//c)$ at high field is observed for data below 25 K for $\Phi = 4 \times 10^{14}$ cm^{-2} and a slightly larger one below 15 K for $\Phi = 2 \times 10^{15}$ cm^{-2}. More obvious is the change of $F_p(H//c)$ shape with a shift of the maximum to 5.5–6 T for a fluence of $\Phi = 2 \times 10^{15}$ cm^{-2}. For $H//ab$ J_c and F_p are progressively suppressed with increasing irradiation over substantially the entire temperature range.

Figure 6 reports a representative example of the angular dependence of J_c at 10 K and 16 T: it shows that the largest increase in J_c is reached after the second irradiation step in an angular range up to 165°. Note that as the field angle approaches that of the *ab*-planes, J_c is suppressed by irradiation. After the third irradiation cycle J_c is significantly suppressed over the entire angular range. The $J_c(\theta)$ curves, measured from 1–16 T, can be rescaled using the Blatter approach [41] with the same anisotropy parameter ($\sim$1.8)[5] before and after irradiation. The dashed lines in figure 6 represent the random pinning contribution, estimated using

---

[5] J_c anisotropy differs from the electronic mass or H_{c2} anisotropies in FBS as a consequence of the multiband-behaviour and the paramagnetic limit as well as possible pinning contribution (see discussion).
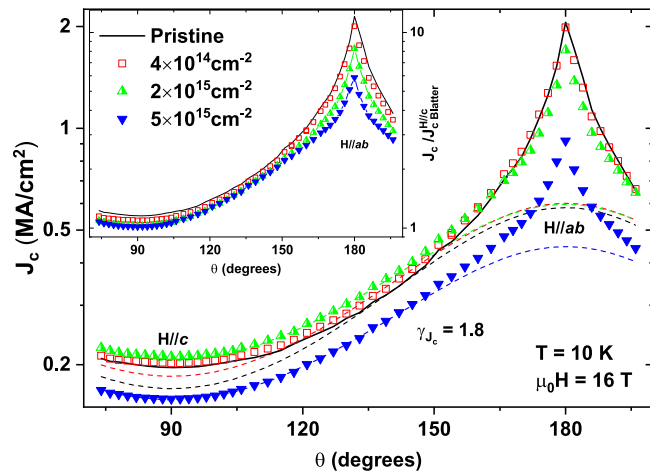
Figure 6. Angular dependence of J_c at 10 K and 16 T for a NdFeAs (O,F) thin film before and after irradiation with α-particles. The dashed lines represent the random pinning contributions as obtained from Blatter rescaling. In the inset, the same data normalized to $J_{c,\text{Blatter}}(H//c)$.

rescaling, whereas the inset presents the same data normalized to $J_{c,\text{Blatter}}(H//c)$. These figures emphasize the effect of the correlated pinning contributions to J_c as the field approaches the *c*-axis and the *ab*-planes.

To better understand the pinning mechanisms contributing before and after irradiation, we analysed the F_p curves for $H//c$ in a wide temperature range with the model introduced in [34] taking into account two superimposed and independent contributions: a interface contribution (*S*) (previously called 'surface' [42]) and a PD one. The *S* contribution is determined by planar defects parallel to the *c*-axis, such as domains, antiphase/twin boundaries and dislocation arrays, whereas PD pinning is likely induced by atomic defects, such as intrinsic PD present in the as-grown sample and the vacancies and interstitial defects artificially introduced by irradiation. This model has four free parameters: two of them define the *S* and PD contribution amplitudes ($F_{p,S}$ and $F_{p,\text{PD}}$) and the other two define their maximum fields of effectiveness (H_S and H_{PD}, the highest of the two corresponding to the irreversibility field). The analysis reveals that H_S and H_{PD} behave differently at low and high temperatures with increasing irradiation (figures 7(a), (b)): at high temperature they decrease with increasing disorder, whereas at low temperature they both show a clear increase. This is particularly obvious for H_{PD}, which increases by ~49% at 10 K (~27% for H_S). However the amplitudes of $F_{p,S}$ and $F_{p,\text{PD}}$ have a different trend (figures 7(c), (d)). $F_{p,S}$ is systematically suppressed with irradiation in the investigated temperature range, whereas $F_{p,\text{PD}}$ is clearly suppressed at high temperature but at 10 K it increases up to 19% at $\Phi = 2 \times 10^{15}\,\text{cm}^{-2}$. This, combined with the increase in H_S and H_{PD}, can lead to a significantly improved performance at larger fields, with J_c extrapolated from the fits improving by 27% at 20 T and almost doubling at 25 T ($\Phi = 2 \times 10^{15}\,\text{cm}^{-2}$). Moreover, extrapolating to lower temperatures, we estimate that a noticeable improvement in the pinning force can be achieved also at low field: in fact at 2 K a maximum F_p of 126 GN m^{-3}

at about 7 T for the pristine sample and 141 GN m^{-3} at 8.3 T for a fluence of $\Phi = 2 \times 10^{15}\,\text{cm}^{-2}$ are expected. The meaning of the insets of figure 7 will be explained in the discussion section.

Since the suppression of $J_c(H//ab)$ with irradiation cannot be ascribed to a change in the J_c anisotropy (Blatter rescaling is performed with the same value), we analyse the *n*-values to better understand the role of irradiation on the film properties when the field approaches the *ab*-planes. The *n*-values are estimated from the *I–V* characteristics that are well described by the $V \propto I^n$ power-law. Figure 8 shows exemplary $n(\theta,H)$ curves at 10 and 20 K for the pristine sample and after irradiations at 2×10^{15} and $5 \times 10^{15}\,\text{cm}^{-2}$ (in figure S1 of the supplementary material, available online at stacks.iop. org/SUST/31/034002/mmedia, we reported 2D plots with data from figure 8 at selected fields). At high temperature (not shown), the $n(\theta)$ curves have a minimum at $H//c$ and a maximum at $H//ab$, similar to the angular dependence of J_c and the data follow the expected $n \sim J_c^\alpha$ relation [34, 43]. At 30–25 K, the sharpness of the *ab*-peak is suppressed and, at 25–20 K, a dip at $H//ab$ appears due to vortex trapping by the Nd-1111 layers and the consequent formation of a vortex-staircase structure [34, 35, 44, 45]. The data at 20 K in figure 8 show this dip (both before and after irradiation) with a flat valley bottom at high field and a small peak emerging in the middle at low field. At 10 K the dip widens and a peak more clearly emerges due to the vortices being locked-in between the layers along the entire sample width [34, 35, 40, 41]. After irradiation, there is a global lowering of the *n*-value and the dip depth and its angular range appears different. To quantify these differences, we estimated the trapping angle $\varphi_T(10\,\text{K}, H)$ as the angle from the *ab*-planes at which the data deviate from $n \sim J_c^\alpha$ [34]. Figure 9(a) shows that the φ_T curves roughly follow the same field dependence, but φ_T progressively decreases with disorder. Subtracting the $n \sim J_c^\alpha$ trend from the $n(\theta)$ curve emphasizes the variation in the dip depth: the data in figure 9(b) and its inset report an example at 10 K and 16 T and it reveals that the dip become more shallow with increasing disorder.

4. Discussion

The normal state behaviour and the superconducting transition observed in the Nd-1111 thin film are very different with respect to what we previously observed on single crystal Nd-1111 [21]. In fact, the latter showed a progressive increase in the normal state resistivity with a clear and significant upturn at low temperatures that was already present after the first irradiation step ($\Phi = 3 \times 10^{15}\,\text{cm}^{-2}$). In contrast, our film shows only a small change in the shape of $\rho(T)$ after a similar irradiation. Also the suppression of T_c by the irradiation is significantly smaller in the film than the single crystal by a factor of ~2.5 (figure 2). The reason for these unexpected differences is uncertain. Since the atom displacements mainly occur on the Nd, Fe and As sites [21] (with the first two elements being magnetic), the upturn observed in the single crystal was ascribed to Kondo-like magnetic scattering
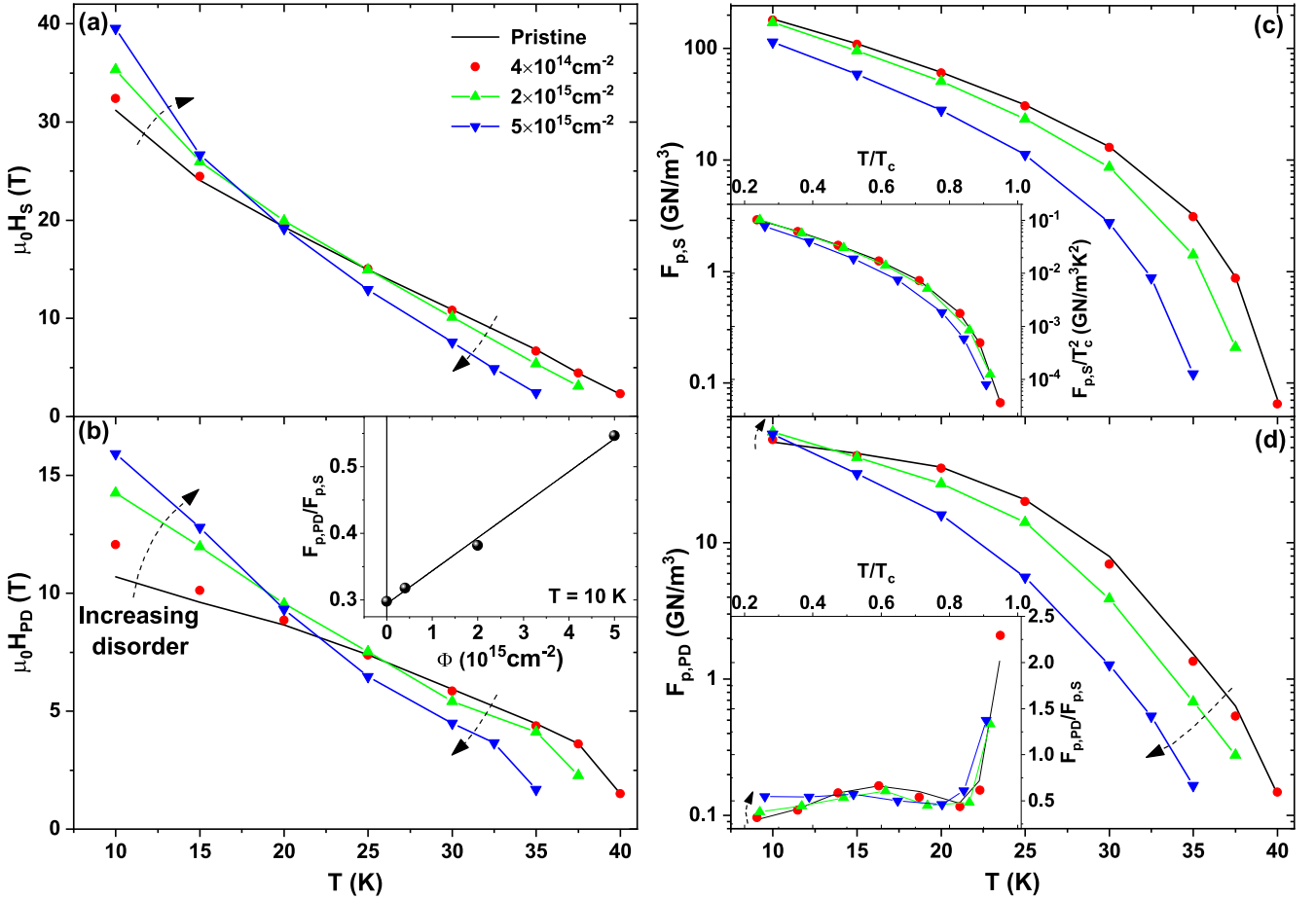
Figure 7. Temperature dependence of the fitting parameters of the $F_p(H//c)$ curves using S ((a) and (c)) and PD ((b) and (d)) contributions for a NdFeAs(O,F) thin film before and after irradiation with α-particles (see text for details). In the inset of panel (c) $F_{p,S}$ normalized to T_c^2 versus the reduced temperature T/T_c. In the inset of panel (d) the ratio between the PD and the S amplitude parameters, $F_{p,\mathrm{PD}}/F_{p,S}$ versus T/T_c. In the inset of panel (b) $F_{p,\mathrm{PD}}/F_{p,S}$ at 10 K as a function of the fluence Φ.

induced by irradiation defects [21]. A possible explanation for the unexpected differences of the post-irradiation properties could be a result of their different doping levels. Since the underdoped single crystal is closer to the antiferromagnetic phase characteristic of Fe-based superconductors [46, 47], it may be more susceptible to magnetic disorder induced by irradiation defects and thus it could induce local off-stoichiometric regions, allowing antiferromagnetism to re-emerge at a much lower level of disorder. Another possible explanation is that in the film the substrate presence and the induced strain prevent the structure from fully relaxing after an irradiation displacement occurs; this could facilitate an increased rate of interstitial-vacancy recombination, partially recovering the disorder.

In regard to H_{c2} and the coherence lengths, we observe different behaviours depending on the field orientations. For $H//c$ the H_{c2} slope monotonically increases (and $\xi_{ab}(0)$ decreases) with irradiation, implying that the dirty limit regime is immediately established (the dirty limit is reached when the mean free path is comparable with the coherence length [48]). For $H//ab$, the slope is unchanged after the first two irradiation cycles (for $T_c \geqslant 48$ K) and then it suddenly increases after the third cycle. This means that a larger level

of disorder is necessary to establish the dirty limit in this orientation: this is not surprising considering that the *c*-axis coherence length is about four times smaller than along *ab*. These different coherence length behaviours generate an unusual trend of γ (figure 4 inset) that in other materials typically decrease with increasing disorder: for instance a monotonic decrease of γ was demonstrated in neutron and α-particle irradiated MgB$_2$ [12, 49], in heavy-ion irradiated iron-based superconductors [50] and in YBCO with spherical nanoparticle [51].

The J_c and F_p performances of the pristine sample are significantly better, by a factor of two to three, than the previously reported results [34]. What is surprising for the present thin film is the ineffectiveness of the new pinning centres in increasing J_c after irradiation. Even more, comparing $J_c(\theta)$ before and after irradiation with their respective random contributions (figure 6) reveals that the *c*-axis correlated pinning present in the pristine sample almost disappears at $\Phi = 2 \times 10^{15}$ cm^{-2}. A possible reason for the reduction of the *c*-axis correlated pinning is that segregation of PD (referred as Cottrell clouds) near planar defects is often found after irradiation as a result of the presence of both
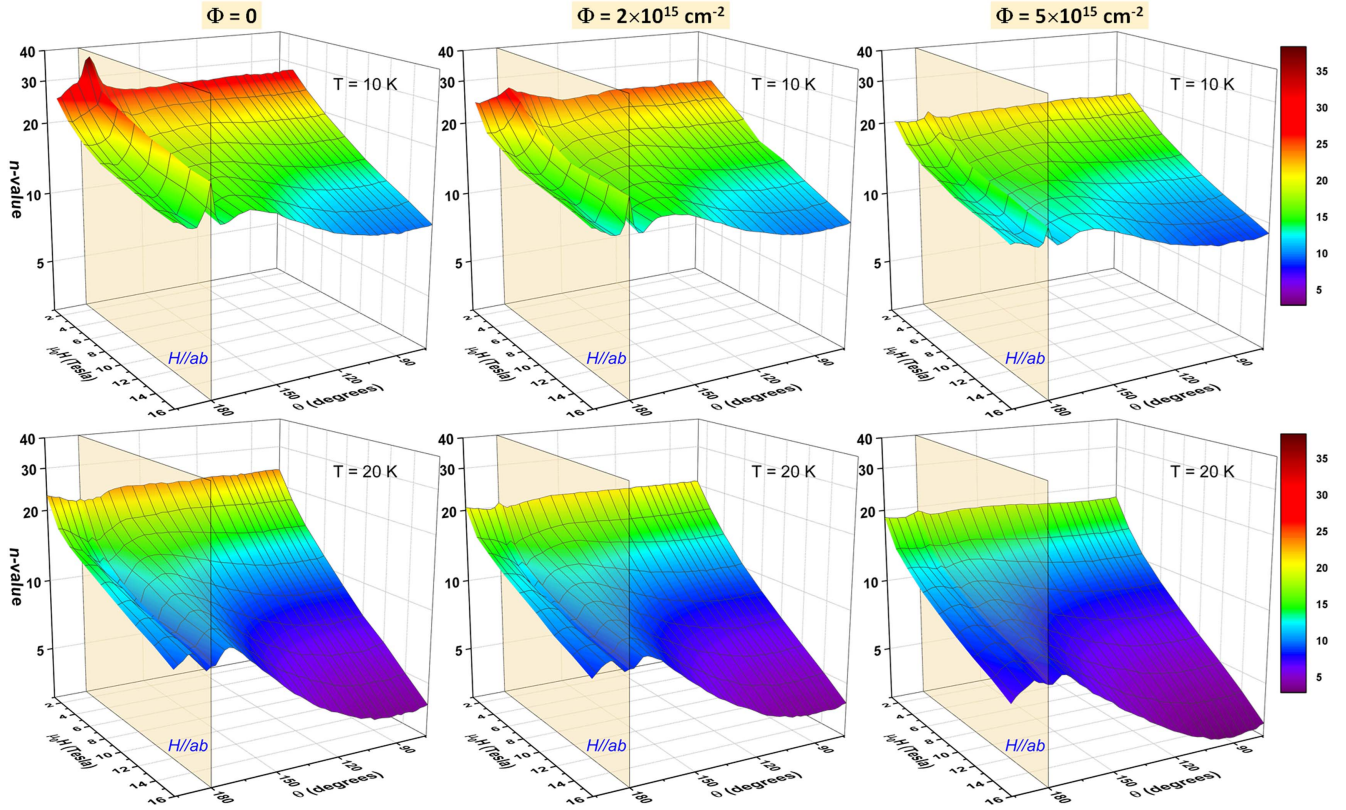
Figure 8. Angular and field dependence of the *n*-values at 10 (first row) and 20 K (second row) for a NdFeAs(O,F) thin film before irradiation (left) and after irradiation at $\Phi = 2 \times 10^{15} \, \text{cm}^{-2}$ (middle) and $\Phi = 5 \times 10^{15} \, \text{cm}^{-2}$ (right).

compressive and tensile strain in the region and the presence of some dangling bonds.

As previously reported, the NdFeAs(O,F) case differs from other 1111 phases. For instance, in the case of LaFeAs (O,F) [52] the H_{c2} and J_c anisotropies assume the same value and have the same temperature dependence. Instead, in NdFeAs(O,F) γ is about 4 near T_c whereas γ_{J_c} is 1.8 at low temperature and it decreases with increasing temperature [34], similarly to what actually found in the Fe(Se,Te) [53]. The reasons for those differences in value and temperature dependence is not completely understood and behind the purpose of this paper but it is likely to be related to the multiband scenario.

The two-contribution pinning model allows us to better understand the J_c and F_p behaviours. The decrease of the H_S and H_{PD} parameters at high temperature with increasing disorder (figure 7) is clearly related to the T_c suppression, whereas their low-temperature increase is due to the enhancement of the low-temperature H_{c2} extrapolation, as inferred from figure 3, and to the increase of PD density in the case of H_{PD}. The amplitudes $F_{p,S}$ and $F_{p,PD}$ in general can be expressed it terms of fundamental and microstructure-related parameters as follows [38, 54]:

$$F_{p,S} = \mu_0 S_v H_c^2 / 2 = S_v E_c, \tag{1}$$

$$F_{p,PD} = \mu_0 V_t H_c^2 / 2.32 a = V_t E_c / 1.16 a, \tag{2}$$

where μ_0 is the vacuum magnetic permittivity, H_c is the thermodynamic critical field, S_v is the pinning surface area per

unit volume projected in the direction of the Lorentz force, a is the average effective diameter of PD, V_t is the fraction of flux-lines length inside the pinning centre and $E_c = \mu_0 H_c^2 / 2$ is the condensation energy that is proportional to $N^* T_c^2$ (with N^* being the renormalized electronic DOS) [47]. Since the microstructure-related parameter S_v for planar defects does not change with irradiation, $F_{p,S}$ in equation (1) should rescale with T_c^2 if N^* remains constant. The inset of figure 7(c) reports the $F_{p,S}$ data normalized to T_c^2 as a function of the reduced temperature T/T_c; it reveals that the curves obtained at 4×10^{14} and $2 \times 10^{15} \, \text{cm}^{-2}$ fluences follow the same trend as the pristine sample, whereas the $5 \times 10^{15} \, \text{cm}^{-2}$ curve clearly falls below the others. This means that up to $\Phi = 2 \times 10^{15} \, \text{cm}^{-2}$, $F_{p,S}$ only changes because of the T_c suppression but after the last irradiation cycle also the DOS is reduced, provoking a significant drop in J_c. A similar rescaling does not work for the PD contribution (not shown): although, taking into account equation (2), this is expected because the increasing PD density with irradiation changes V_t, we also observe a change in the curve temperature dependences. The inset of figure 7(d) helps to better understand how the PD contribution changes with irradiation: it shows the reduced temperature dependence of the amplitude ratio, $F_{p,PD}/F_{p,S}$, that is independent from the condensation energy and equal to $V_t / 1.16 a S_v$. All curves have a maximum approaching T_c, a sort of plateau at intermediate temperature, but they separate at the lowest temperatures. In fact $F_{p,PD}/F_{p,S}(10 \, \text{K})$ almost doubles after the final cycle with
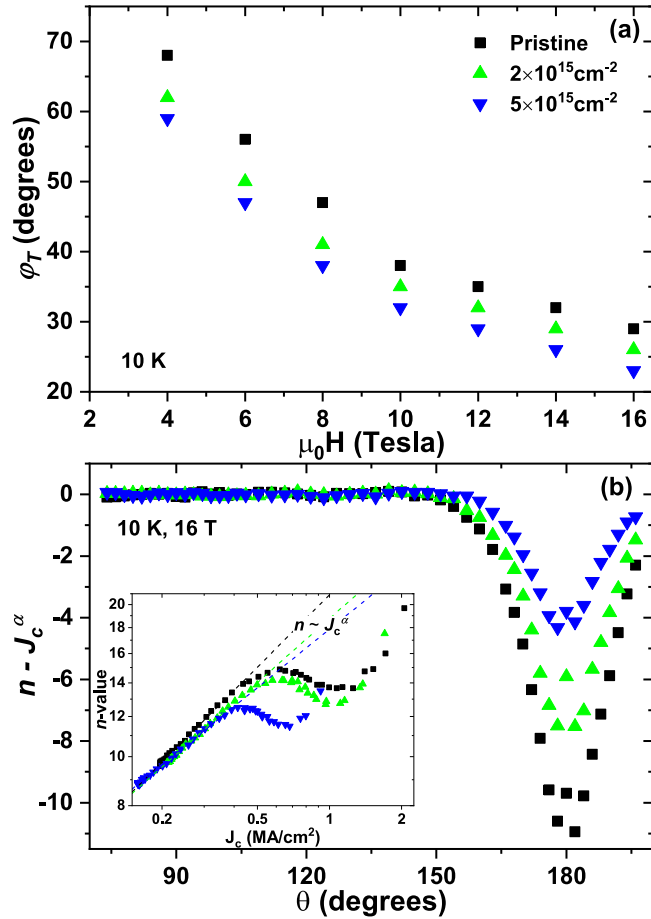
Figure 9. (a) Trapping angles as a function of applied field at 10 K for a NdFeAs(O,F) thin film before and after irradiation with α-particles. (b) Angular dependence of $n - J_c^\alpha$ obtained by subtracting the power-law behaviour found in the $n(J_c)$ plot (see inset) from the n-value (at 10 K and 16 T).

respect to the pristine sample. If L is the average distance between pinning centres, V_t can vary from $(a/L)^3$ in the case of rigid vortices to (a/L) in the case of perfectly flexible vortices or when $L \sim d$, with d being the vortex spacing (matching effect) [38]; $F_{p,PD}/F_{p,S}$ assumes values between:

$$F_{p,PD}/F_{p,S} = a^2/1.16S_v L^3 = 1/1.16S_v L(a/L)^2$$
$$\text{for rigid vortices} \qquad (3)$$

$$\text{and} \quad F_{p,PD}/F_{p.S} = 1/1.16S_v L$$
$$\text{perfectly flexible vortices (or } L \sim d). \qquad (4)$$

To verify these relations in the inset of figure 7(b), we plot the $F_{p,PD}/F_{p,S}$ at 10 K as a function of the fluence Φ, which is proportional to $(1/L)^3$: at low temperature all PD (either pre-existing or induced by irradiation) should be effective pinning centres. $F_{p,PD}/F_{p,S}$ versus Φ shows a roughly linear trend indicating that at this temperature $F_{p,PD}/F_{p,S}$ follows relation (3) and the vortices are rigid [$V_t \sim (a/L)^3$], as predicted by Dew-Hughes [42]. We can also note that, at $\Phi = 0$, $F_{p,PD}/F_{p,S}$ does not go to 0 as a result of the presence of pre-existing defects. When approaching T_c (figure 7(d) inset), $F_{p,PD}/F_{p,S}$ increases toward the limiting value in equation (4) as a result of the increased flexibility of

the vortex and the smaller applied fields, that are close to the matching field. At intermediate temperatures ($T/T_c \sim$ 0.5–0.85), the small variations in $F_{p,PD}/F_{p,S}$ are probably due to some PD gradually losing effectiveness with increasing ξ (T) and, as a consequence, changing the a/L ratio in equation (3).

The n-value carries information about the pinning performance properties through the relation $n \sim U_p/k_B T$ (with U_p being the pinning potential and k_B the Boltzmann constant) [35, 55]. In the pristine sample at low temperature, when the vortex-staircase forms, the segments of vortices (kinks) connecting the trapped parts are not or are weakly pinned and they can easily move due to the Lorentz force being almost parallel to the ab-planes [34, 40]: this leads to the n-value suppression and to the formation of the $n(\theta)$ dip when the field orientation approaches the ab-planes. When the field orientation is even closer to the ab-planes, the length of the trapped segments of the vortices becomes comparable with the sample width and the vortices become fully locked parallel to the ab-planes, generating the sudden increase in the n-value and the formation of the peak inside the dip. Clearly a similar effect occurs also after irradiation, but the progressive decrease of φ_T and the dip shallowness with increasing irradiation are surprising. φ_T is related to γ (and so to $\xi_c = \xi_{ab}/\gamma$) [38] and the monotonic trend of φ_T with disorder is inconsistent with the non-monotonic behaviour of γ shown in figure 4. The small increase of ξ_c at $\Phi = 2 \times 10^{15}$ cm^{-2} leads to a small decrease of φ_T (as expected) but the following strong ξ_c suppression at $\Phi = 5 \times 10^{15}$ cm^{-2} should produce a clear increase of φ_T due to the vortices being trapped over a wider angle around the ab-planes. The reason this increase of φ_T does not occur and the dip becomes less pronounced is likely related to the increased density of PD. In fact, the PD introduced by irradiation are likely able to partially prevent the movement of the vortex kinks: as a consequence, although the staircase-structure forms, the vortex movement is inhibited until the field is aligned closer to the ab-planes (smaller φ_T with increasing disorder) and the n-value dip is suppressed due to the additional pinning centres (smaller deviation from the $n \sim J_c^\alpha$ trend with increasing disorder). Moreover it is possible that pinning by PD competes with the intrinsic pinning produced by the Nd-1111 layered structure, preventing the development of long vortex lengths lying parallel to the ab-planes and reducing the effect of intrinsic pinning in the formation of a sharp J_c ab-peak.

5. Conclusions

Here we show that, despite the rather limited T_c suppression upon α-particle irradiation of Nd-1111, H_{c2} and H_{irr} can be significantly enhanced by radiation-induced disorder. In contrast to the typically found monotonic irradiation-induced decrease in the electronic anisotropy found in most superconductors, we found an initial decrease of γ with increasing disorder, then followed by a sharp increase. The effects of irradiation disorder on J_c depend on the field orientation. PD flux-pinning centres are indeed introduced in the system

proportionally to α-particle fluence. However irradiation actually suppress the c-axis correlated pinning contribution by suppressing T_c and by reducing the DOS. When the applied magnetic field approaches the ab-planes, the J_c is reduced over the whole temperature range as a result of the competition between the PD and intrinsic pinning mechanisms. Our results indicate that irradiation can improve the performance of Nd-1111 at high field and lower temperature and that it also can reduce the effective J_c anisotropy.

Acknowledgments

ORCID iDs

C Tarantini ⓘ https://orcid.org/0000-0002-3314-5906
K Iida ⓘ https://orcid.org/0000-0003-1038-9630
T Hatano ⓘ https://orcid.org/0000-0003-2315-8487
H Ikuta ⓘ https://orcid.org/0000-0003-1522-7091
R K Singh ⓘ https://orcid.org/0000-0002-4498-0800
N Newman ⓘ https://orcid.org/0000-0003-2819-9616

References

[1] Poate J M, Dynes R C, Testardi L R and Hammond R H 1976 Comments on defect production and stoichiometry in A-15 superconductors *Phys. Rev. Lett.* **37** 1308

[2] Viswanathan R and Caton R 1978 Effect of neutron irradiation on single-crystal V_3Si: heat capacity and resistivity *Phys. Rev. B* **18** 15

[3] Cort B, Stewart G R, Snead C L Jr, Sweedler A R and Moehlecke S 1981 Specific-heat studies of neutron-irradiated A15 Nb_3Al *Phys. Rev. B* **24** 3794

[4] Wiesmann H, Gurvitch M, Ghosh A K, Lutz H, Kammerer O F and Strongin M 1978 Estimate of density-of-states changes with disorder in A-15 superconductors *Phys. Rev. B* **17** 122

[5] Ghosh A K, Gurvitch M, Wiesmann H and Strongin M 1978 Density of states in two A-15 materials *Phys. Rev. B* **18** 6116

[6] Spina T, Scheuerlein C, Richter D, Bordini B, Bottura L, Ballarino A and Flükiger R 2015 Variation of the critical properties of alloyed Nb–Sn wires after proton irradiation at 65 and 24 GeV *IEEE Trans. Appl. Supercond.* **25** 6000505

[7] Baumgartner T, Eisterer M, Weber H W, Flükiger R, Scheuerlein C and Bottura L 2014 Effects of neutron irradiation on pinning force scaling in state-of-the-art Nb_3Sn wires *Supercond. Sci. Technol.* **27** 015005

[8] Putti M, Affronte M, Ferdeghini C, Manfrinetti P, Tarantini C and Lehmann E 2006 Observation of the crossover from two-gap to single-gap superconductivity through specific heat measurements in neutron-irradiated MgB_2 *Phys. Rev. Lett.* **96** 077003

[9] Daghero D, Calzolari A, Ummarino G A, Tortello M, Gonnelli R S, Stepanov V A, Tarantini C, Manfrinetti P and Lehmann E 2006 Point-contact spectroscopy in neutron-irradiated $Mg^{11}B_2$ *Phys. Rev. B* **74** 174519

[10] Eisterer M, Zehetmayer M and Weber H W 2003 Current percolation and anisotropy in polycrystalline MgB_2 *Phys. Rev. Lett.* **90** 247002

[11] Wilke R H T, Bud'ko S L, Canfield P C, Farmer J and Hannahs S T 2006 Systematic study of the superconducting and normal-state properties of neutron-irradiated MgB_2 *Phys. Rev. B* **73** 134512

[12] Gandikota R *et al* 2005 Effect of damage by 2 MeV He ions and annealing on H_{c2} in MgB_2 thin films *Appl. Phys. Lett.* **87** 072507

[13] Tarantini C *et al* 2016 Effects of neutron irradiation on polycrystalline $Mg^{11}B_2$ *Phys. Rev. B* **73** 134518

[14] Rullier-Albenque F, Alloul H and Tourbot R 2001 Disorder and transport in cuprates: weak localization and magnetic contributions *Phys. Rev. Lett.* **87** 157001

[15] Krusin-Elbaum L, Civale L, Blatter G, Marwick A D, Holtzberg F and Field C 1994 Bose-glass melting in YBaCuO crystals with correlated disorder *Phys. Rev. Lett.* **72** 1914

[16] Petrean A M, Paulius L M, Kwok W K, Fendrich J A and Crabtree G W 2000 Experimental evidence for the vortex glass phase in untwinned, proton irradiated $YBa_2Cu_3O_{7-\delta}$ *Phys. Rev. Lett.* **84** 5852

[17] Civale L, Marwick A D, Worthington T K, Kirk M A, Thompson J R, Krusin-Elbaum L, Sun Y, Clem J R and Holtzberg F 1991 Vortex confinement by columnar defects in $YBa_2Cu_3O_7$ crystals: enhanced pinning at high fields and temperatures *Phys. Rev. Lett.* **67** 648

[18] Matsui H, Ogiso H, Yamasaki H, Kumagai T, Sohma M, Yamaguchi I and Manabe T 2012 4-fold enhancement in the critical current density of $YBa_2Cu_3O_7$ films by practical ion irradiation *Appl. Phys. Lett.* **101** 232601

[19] Jia Y *et al* 2013 Doubling the critical current density of high temperature superconducting coated conductors through proton irradiation *Appl. Phys. Lett.* **103** 122601

[20] Karkin A E, Werner J, Behr G and Goshchitskii B N 2009 Neutron-irradiation effects in polycrystalline $LaFeAsO_{0.9}F_{0.1}$ superconductors *Phys. Rev. B* **80** 174512

[21] Tarantini C *et al* 2010 Suppression of the critical temperature of superconducting NdFeAs(OF) single crystals by Kondo-like defect sites induced by α-particle irradiation *Phys. Rev. Lett.* **104** 087002

[22] Nakajima Y, Taen T, Tsuchiya Y, Tamegai T, Kitamura H and Murakami T 2010 Suppression of the critical temperature of superconducting $Ba(Fe_{1-x}Co_x)_2As_2$ by point defects from proton irradiation *Phys. Rev. B* **82** 220504

[23] Prozorov R, Kończykowski M, Tanatar M A, Thaler A, Bud'ko S L, Canfield P C, Mishra V and Hirschfeld P J 2014 Effect of electron irradiation on superconductivity in single crystals of $Ba(Fe_{1-x}Ru_x)_2As_2$ ($x = 0.24$) *Phys. Rev. X* **4** 041032

[24] Schilling M *et al* 2016 Tracing the $s_\pm$ symmetry in iron pnictides by controlled disorder *Phys. Rev. B* **93** 174515

[25] Nakajima Y, Tsuchiya Y, Taen T, Tamegai T, Okayasu S and Sasase M 2009 Enhancement of critical current density in Co-doped $BaFe_2As_2$ with columnar defects introduced by heavy-ion irradiation *Phys. Rev. B* **80** 012510

[26] Fang L *et al* 2012 High, magnetic field independent critical currents in $(Ba,K)Fe_2As_2$ crystals *Appl. Phys. Lett.* **101** 012601

[27] Maiorov B, Katase T, Usov I O, Weigand M, Civale L, Hiramatsu H and Hosono H 2012 Competition and cooperation of pinning by extrinsic point-like defects and intrinsic strong columnar defects in $BaFe_2As_2$ thin films *Phys. Rev.* B **86** 094513

[28] Eisterer M, Mishev V, Zehetmayer M, Zhigadlo N D, Katrych S and Karpinski J 2014 Critical current anisotropy in Nd-1111 single crystals and the influence of neutron irradiation *Supercond. Sci. Technol.* **27** 044009

[29] Eisterer M, Weber H W, Jiang J, Weiss J D, Yamamoto A, Polyanskii A A, Hellstrom E E and Larbalestier D C 2009 Neutron irradiation of $SmFeAsO_{1-x}F_x$ *Supercond. Sci. Technol.* **22** 065015

[30] Eisterer M, Raunicher R, Weber H W, Bellingeri E, Cimberle M R, Pallecchi I, Putti M and Ferdeghini C 2011 Anisotropic critical currents in $FeSe_{0.5}Te_{0.5}$ films and the influence of neutron irradiation *Supercond. Sci. Technol.* **24** 065016

[31] Ozaki T, Wu L, Zhang C, Jaroszynski J, Si W, Zhou J, Zhu Y and Li Q 2016 A route for a strong increase of critical current in nanostrained iron-based superconductors *Nat. Commun.* **7** 13036

[32] Kawaguchi T, Uemura H, Ohno T, Tabuchi M, Ujihara T, Takeda Y and Ikuta H 2011 Molecular beam epitaxy growth of superconducting NdFeAs(O,F) thin films using a F-getter and a novel F-doping method *Appl. Phys. Express* **4** 083102

[33] Uemura H, Kawaguchi T, Ohno T, Tabuchi M, Ujihara T, Takeda Y and Ikuta H 2012 Substrate dependence of the superconducting properties of NdFeAs(O,F) thin films *Solid State Commun.* **152** 735

[34] Tarantini C *et al* 2016 Intrinsic and extrinsic pinning in NdFeAs(O,F): vortex trapping and lock-in by the layered structure *Sci. Rep.* **6** 36047

[35] Fuchs G *et al* 2009 Orbital and spin effects for the upper critical fields in As-deficient disordered Fe pnictide superconductors *New J. Phys.* **11** 075007

[36] Gurevich A 2011 Iron-based superconductors at high magnetic fields *Rep. Prog. Phys.* **74** 124501

[37] Tarantini C, Gurevich A, Jaroszynski J, Balakirev F, Bellingeri E, Pallecchi I, Ferdeghini C, Shen B, Wen H H and Larbalestier D C 2011 Significant enhancement of upper critical fields by doping and strain in iron-based superconductors *Phys. Rev.* B **84** 184522

[38] Blatter G, Feigl'man M, Geshkenbin V B, Larkin A I and Vinokur V 1994 Vortices in high-temperature superconductors *Rev. Mod. Phys.* **66** 1125

[39] Werthamer N R, Helfard E and Hohenberg P C 1966 Temperature and purity dependence of the superconducting critical field, H_{c2}: III. Electron spin and spin–orbit effects *Phys. Rev.* **147** 295

[40] Weyeneth S, Puzniak R, Zhigadlo N D, Katrych S, Bukowski Z, Karpinski J and Keller H 2009 Evidence for two distinct anisotropies in the oxypnictide superconductors $SmFeAsO_{0.8}F_{0.2}$ and $NdFeAsO_{0.8}F_{0.2}$ *J. Supercond. Nov. Magn.* **22** 347

[41] Blatter G, Geshkenbein V B and Larkin A I 1992 From isotropic to anisotropic superconductors: a scaling approach *Phys. Rev. Lett.* **68** 875

[42] Dew-Hughes D 1974 Flux pinning mechanisms in type II superconductors *Phil. Mag.* **30** 293

[43] Opherden L *et al* 2016 Large pinning forces and matching effects in $YBa_2Cu_3O_{7-\delta}$ thin films with $Ba_2Y(Nb/Ta)O_6$ nano-precipitates *Sci. Rep.* **6** 21188

[44] Kwok W K, Welp U, Vinokur V M, Fleshler S, Downey J and Crabtree G W 1991 Direct observation of intrinsic pinning by layered structure in single-crystal $YBa_2Cu_3O_{7-\delta}$ *Phys. Rev. Lett.* **67** 390

[45] Civale L *et al* 2004 Influence of crystalline texture on vortex pinning near the *ab*-plane in $YBa_2Cu_3O_7$ thin films and coated conductors *Physica* C **412** 976

[46] Hosono H, Tanabe K, Takayama-Muromachi E, Kageyama H, Yamanaka S, Kumakura H, Nohara M, Hiramatsu H and Fujitsu S 2015 Exploration of new superconductors and functional materials, and fabrication of superconducting tapes and wires of iron pnictides *Sci. Technol. Adv. Mater.* **16** 033503

[47] Paglione J and Greene R L 2010 High-temperature superconductivity in iron-based materials *Nat. Phys.* **6** 645

[48] Parks R D 1969 *Superconductivity* vol 2 (New York: Dekker)

[49] Eisterer M, Krutzler C and Weber H W 2005 Influence of the upper critical-field anisotropy on the transport properties of polycrystalline MgB_2 *J. Appl. Phys.* **98** 033906

[50] Fang L *et al* 2013 Huge critical current density and tailored superconducting anisotropy in $SmFeAsO_{0.8}F_{0.15}$ by low-density columnar-defect incorporation *Nat. Commun.* **4** 2655

[51] Malmivirta M, Palonen H, Inkinen S, Yao L D, Tikkanen J, Huhtinen H, Jha R, Awana V P S, van Dijken S and Paturi P 2016 Dirty limit scattering behind the decreased anisotropy of doped $YBa_2Cu_3O_{7-\delta}$ thin films *J. Phys.: Condens. Matter* **28** 175702

[52] Kidszun M, Haindl S, Thersleff T, Hänisch J, Kauffmann A, Iida K, Freudenberger J, Schultz L and Holzapfel B 2011 Critical current scaling and anisotropy in oxypnictide superconductors *Phys. Rev. Lett.* **106** 137001

[53] Iida K *et al* 2013 Intrinsic pinning and the critical current scaling of clean epitaxial Fe(Se,Te) thin films *Phys. Rev.* B **87** 104510

[54] Pallecchi I *et al* 2005 Enhanced flux pinning in neutron irradiated MgB_2 *Phys. Rev.* B **71** 212507

[55] Zeldov E, Amer N M, Koren G, Gupta A, McElfresh M W and Gambino R J 1990 Flux creep characteristics in high-temperature superconductors *Appl. Phys. Lett.* **56** 680